

Robust Nonlinear Controller to Damp Drivetrain Torsional Oscillation of Wind Turbine Generators

Bi Liu, Junbo Zhao, *Senior Member, IEEE*, Qi Huang, *Senior Member, IEEE*, Federico Milano, *Fellow, IEEE*, Weihao Hu, *Senior Member, IEEE*

Abstract—This paper develops a novel nonlinear controller for the mitigation of drivetrain torsional oscillations of wind turbine generators following large disturbances. The key idea is to integrate differential geometry theory with an extended state observer. Differential geometry allows transforming the wind turbine generator nonlinear model into a simple second-order Brunovsky system, whereas the extended state observer can accurately estimate the states of the transformed Brunovsky system and compensate unknown disturbances. Simulation results show that, under various conditions in different test systems, the proposed controller achieves significant enhancements with respect to conventional approximate linearization-based controller and nonlinear sliding mode control-based method.

Index Terms—Drivetrain torsional oscillation, extended state observer, nonlinear controller, power system dynamics, power system stability control, wind turbine generator.

NOMENCLATURE

C	Capacitance of DC bridge
D_{sh}	Damping coefficient of WTG drivetrain
H_g	Inertia constant of wind generator in second
H_t	Inertia constant of the wind turbine in second
K_{sh}	Stiffness coefficient of WTG drivetrain
i_{dr}	d -axis current of wind generator rotor
i_{ds}	d -axis current of wind generator stator
i_{qr}	q -axis current of wind generator rotor
i_{qs}	q -axis current of wind generator stator
L_m	Mutual inductance between wind generator stator and rotor
L_r	Self inductance of wind generator rotor
L_s	Self inductance of wind generator stator
R_r	Resistance of wind generator rotor
R_s	Resistance of wind generator stator
T_e	Electromagnetic torque of wind generator
T_m	Mechanical torque of wind generator
v_{dc}	Voltage of DC bridge
v_{dr}	d -axis voltage of wind generator rotor
v_{ds}	d -axis voltage of wind generator stator
v_{qr}	q -axis voltage of wind generator rotor
v_{qs}	q -axis voltage of wind generator stator

V_{cutin}	The cut-in wind speed of WTG
V_{cutout}	The cut-out wind speed of WTG
V_{rated}	The rated wind speed of WTG
θ_{sh}	Torsional angle between the wind turbine and generator rotor
λ_{dr}	d -axis flux of wind generator rotor
λ_{ds}	d -axis flux of wind generator stator
λ_{qr}	q -axis flux of wind generator rotor
λ_{qs}	q -axis flux of wind generator stator
ω	Angular velocity of the rotating dq reference frame
ω_B	Nominal angular velocity of WTG rotor
ω_g	Angular velocity of wind generator rotor in rad/s
ω_{wt}	Angular velocity of wind turbine

I. INTRODUCTION

The integration of wind generators into power system has significantly increased in the past two decades [1]. This brings several challenges for secure system operation and control. Among these, the drivetrain torsional oscillation (DTTO) of wind turbine generator (WTG) is a particularly relevant phenomenon in the presence of large disturbances. Since the model of wind turbine equivalent shaft is relatively softer than the practical turbine shaft [2], the drivetrain of the wind turbine should be described with a two-mass model [3], or three-mass model [4]. Therefore, there exists the phenomenon of WTG DTTO. The DTTO of WTG is mainly caused by (i) the perturbations of electromagnetic torque following a grid-side fault [5]–[7] or the ancillary frequency support provided by the wind power plants [8], [9]; and (ii) the sudden variations of the mechanical torque of WTG resulted from the intrinsic intermittent behavior of wind speed [10]. If not properly damped, DTTO causes the mechanical fatigue of WTG drivetrain, leading to a significant reduction of WTG service life. This in turn causes economic losses and system security concern.

FACTS devices can be used to damp WTG DTTO [11], [12]. For instance, a gate-controlled series capacitor containing a pair of switches in parallel with a capacitor can help damp DTTO via adjusting the effective reactance of transmission line [11]. However, this only works for the DTTO resulted from variations of the electromagnetic torque of the WTG, such as a grid fault. DTTO caused by the change of mechanical torque, such as the wind speed variations, cannot be addressed with this technique.

Various torque compensation-based methods for WTG via the converters have been developed, aiming at providing damping torque, inertial torque, or other compensation torque

This research work is supported by The National Key Research and Development Program of China (2017YFB0902002) and Technology Project of State Grid (SGXJ0000KXJS1700841).

B. Liu, Q. Huang and W. Hu are with the Sichuan Provincial Key Lab Science and Technology of China, Chengdu, Sichuan, 611731, PR China. (e-mail: liubi_2006@126.com; hwong@uestc.edu.cn, whu@uestc.edu.cn).

J. Zhao is with Department of Electrical and Computer Engineering, Mississippi State University, Starkville, MS 39762, USA (junbo@ece.msstate.edu).

F. Milano is with the School of Electrical and Electronic Engineering, University College Dublin, Dublin, Ireland (e-mail: federico.milano@ucd.ie).

by means of reactive power modulation. The additional torque is superimposed to the normal electromagnetic torque for the mitigation of WTG DTTO. In [13], a small ripple at the drivetrain frequency is added to the generator torque control and the effect of the resonance is counteracted by the adjusted phase, leading to the improvement on oscillation damping. Torsional oscillations caused by a grid fault are significant if no damping controller is in place. To deal with this issue, [5] proposes a model-based active damping controller for the torsional vibration using the linear-quadratic-Gaussian (LQG) algorithm. The damping control for the torsional oscillations can be done with STATCOM/BESS as well [6]. [7] develops a control scheme for active oscillation damping of WTG, where a corrective signal is obtained from the torque damping controller and further added to the reference torque such that the DTTO of WTG is reduced. [10] investigates the drivetrain dynamics under different operating regions of the power-speed curve and develops a DFIG drivetrain stabilizer, where additional damping torque is achieved by a state feedback from the rotor speed to the referenced electromagnetic power. In [14], a band-trap filter is proposed to eliminate periodic torque disturbance of the generator torque control loop. This enables the controller to weaken the exciting input of the drivetrain and subsequently damp the DTTO. In [15], [16], a virtual inertial controller is developed for DTTO mitigation, where the first-order derivative of the angular speed about wind generator rotor is used as the input signal to provide an additional electromagnetic torque component via the generator-side converter. In [17], a torsional oscillation damping control scheme based on model predictive control is proposed. With the state feedback control strategy and the model-based torque estimation, the controller compensates shaft torque difference of WTG at the torsional frequency for the active damping of DTTO. In order to maximize the energy production of WTG without fatigue damages induced by torsional vibration within the drivetrain subsystem, a receding horizon optimal control framework [18] is developed. Note that the ancillary frequency control of WTG may induce DTTO or deteriorate their damping [9]. To this end, an adaptive damping control scheme based on reactive power modulation of WTG is proposed in [19]. By means of modulating active current component of WTG, a damping torque is produced according to the drivetrain speed [20].

The aforementioned methods are mainly developed on the first order Taylor series expansion approximation around its equilibrium point. However, the truncation of the Taylor series expansion may result in large error in the presence of large disturbances. To solve this issue, a nonlinear controller called sliding mode control (SMC) has been adopted for the mitigation of DTTO [21]. SMC is able to damp DTTO following a large disturbance but suffers from the well-known chattering phenomenon caused by its discontinuous behavior [22]. It is worth noting that SMC is likely one of the most effective nonlinear control techniques in the literature that are able to handle the WTG DTTO following large disturbances. Actually, an effective approach for dealing with such issue is the nonlinear control theory [23].

In the past decades, differential geometry theory [24] has

been widely applied into nonlinear control [25]. Relevant engineering applications of this theory are robot arm control [26], automatic flight control [27] and power systems [28], [29]. The key idea of differential geometry-based nonlinear control is to transform the original nonlinear system into a completely or partially cascade integral system by calculating Lie derivatives. However, differential geometry poses a significant challenge of computational complexity for systems whose mathematical model exceeds the third order. Furthermore, since such controller is in fact related to the system parameters, it does not have good capability of being resistance to model parameter uncertainties. Coincidentally, the extended state observer (ESO) has the ability of directly estimating a cascade integral system according to the system output function without relying on the system parameters, and simultaneously accounting for the external disturbance [30].

This paper aims to develop a new controller to damp WTG DTTO originated by large disturbances. The specific contributions of this paper are as follows:

- Motivated by differential geometry theory, the nonlinear WTG integrated system can be transformed into a simple second-order Brunovsky system via a nonlinear coordinate transformation. This allows designing a state feedback-based nonlinear controller of the transformed second-order Brunovsky system. It significantly reduces the complexity of the controller and, at the same time, circumvents the large truncation error that occurs in conventional approximate linearization-based controllers.
- An ESO is developed to estimate the states of the second-order Brunovsky system and the overall disturbance, including the uncertainties of model parameters and the external disturbance. This highly reduces the computational burden of the calculation of Lie derivatives required by the transformation above and significantly enhances the performance in suppressing the WTG DTTO by effectively compensating the disturbances.

The proposed controller has the following features: (i) leads to a simple controller; (ii) enhances robustness with respect to WTG model parameter uncertainty; and (iii) damps effectively WTG DTTO in presence of large disturbance. A comprehensive set of test cases and comparisons with conventional approximate linearization-based controllers and SMC-based nonlinear controllers demonstrate the enhanced control performance of the proposed method under various conditions.

The remainder of this paper is organized as follows. In Section II, a nonlinear controller of the WTG is proposed to mitigate DTTO in the presence of large disturbances. Extensive simulation results are carried out and analyzed in Section III. Finally, Section IV draws relevant conclusions and outlines future work.

II. PROPOSED NONLINEAR CONTROLLER OF WTG DTTO

In this section, the ESO is embedded with differential geometry theory to design a novel nonlinear controller. Mathematical derivations are discussed first. Then, the WTG dynamic model is presented, followed by the development of the proposed nonlinear controller.

A. Differential Geometry Theory

Unlike the first-order Taylor series expansion-based linearization that may have large truncation error in the presence of strong nonlinearity, i.e., large disturbance encountered nonlinear system, differential geometry provides the “exact” linearization. It can, in fact, exactly transform a nonlinear system into a linear system or a partial linear system by means of a nonlinear coordinate transformation [31]. Since the former is a special case of the latter, only the partially exact linearization approach is introduced below.

Considering the following nonlinear system:

$$\begin{aligned} \dot{\mathbf{x}} &= \mathbf{f}(\mathbf{x}) + \mathbf{g}(\mathbf{x})u, \\ y &= h(\mathbf{x}), \end{aligned} \quad (1)$$

where $\mathbf{x} \in \mathbb{R}^n$ is the state vector; \mathbf{f} and \mathbf{g} are $n \times 1$ dimensional nonlinear functions of the state and the input, respectively. The output nonlinear function $h(\mathbf{x})$ satisfies:

$$\begin{cases} L_{\mathbf{g}}L_{\mathbf{f}}^i h(\mathbf{x}) = 0 & i < r - 1, \\ L_{\mathbf{g}}L_{\mathbf{f}}^{r-1} h(\mathbf{x}) \neq 0, \end{cases} \quad (2)$$

where $r \leq n$ and $r \in \mathbb{N}$. The operator $L_{\boldsymbol{\eta}(\mathbf{x})}^k \lambda(\mathbf{x})$ denotes the k -order Lie derivative of a scalar field $\lambda(\mathbf{x})$ along with a vector field $\boldsymbol{\eta}(\mathbf{x})$ [32], operating as follows:

$$\begin{cases} L_{\boldsymbol{\eta}(\mathbf{x})} \lambda(\mathbf{x}) = \frac{\partial \lambda(\mathbf{x})}{\partial \mathbf{x}^T} \boldsymbol{\eta}(\mathbf{x}) = \sum_{i=1}^n \frac{\partial \lambda(\mathbf{x})}{\partial x_i} \eta_i(\mathbf{x}), \\ L_{\boldsymbol{\eta}(\mathbf{x})}^2 \lambda(\mathbf{x}) = \frac{\partial L_{\boldsymbol{\eta}(\mathbf{x})} \lambda(\mathbf{x})}{\partial \mathbf{x}^T} \boldsymbol{\eta}(\mathbf{x}), \\ \vdots \\ L_{\boldsymbol{\eta}(\mathbf{x})}^k \lambda(\mathbf{x}) = \frac{\partial L_{\boldsymbol{\eta}(\mathbf{x})}^{k-1} \lambda(\mathbf{x})}{\partial \mathbf{x}^T} \boldsymbol{\eta}(\mathbf{x}). \end{cases} \quad (3)$$

Thus, we have $L_{\mathbf{g}}L_{\mathbf{f}}^i h(\mathbf{x}) = \frac{\partial L_{\mathbf{f}(\mathbf{x})}^i h(\mathbf{x})}{\partial \mathbf{x}^T} \mathbf{g}(\mathbf{x})$.

If one applies the following nonlinear coordinate transformation:

$$\begin{aligned} z_1 &= h(\mathbf{x}), z_2 = L_{\mathbf{f}} h(\mathbf{x}), \dots, z_r = L_{\mathbf{f}}^{r-1} h(\mathbf{x}), \\ z_{r+1} &= \varphi_{r+1}(\mathbf{x}), \dots, z_n = \varphi_n(\mathbf{x}), \end{aligned} \quad (4)$$

where $L_{\mathbf{g}}\varphi_i(\mathbf{x}) = 0$ ($r+1 \leq i \leq n$, $n \in \mathbb{N}$) holds, the original nonlinear system (1) can be transformed into:

$$\begin{aligned} \dot{z}_1 &= z_2, \dot{z}_2 = z_3, \dots, \dot{z}_r = a(\mathbf{x}) + b(\mathbf{x})u, \\ \dot{z}_{r+1} &= q_{r+1}(\mathbf{x}), \dots, \dot{z}_n = q_n(\mathbf{x}), \end{aligned} \quad (5)$$

where $a(\mathbf{x}) = L_{\mathbf{f}}^r h(\mathbf{x})$, $b(\mathbf{x}) = L_{\mathbf{g}}L_{\mathbf{f}}^{r-1} h(\mathbf{x})$, and $q_i(\mathbf{x}) = \dot{\varphi}_i(\mathbf{x})$ ($r+1 \leq i \leq n$).

Note that if one lets $a(\mathbf{x}) + b(\mathbf{x})u = \xi$, the first r equations of (5) form a simple Brunovsky standard system, which is a completely controllable linear system in the cascade integral form. Hence, the linear control theory, such as the linear quadratic optimal theory [33] can be adopted to obtain ξ

$$\xi = \sum_{j=1}^r -k_j z_j \quad (6)$$

Thus, the control strategy of the nonlinear system (1) can be derived as:

$$u = \frac{-a(\mathbf{x}) - \sum_{j=1}^r k_j z_j}{b(\mathbf{x})}. \quad (7)$$

In order to obtain (4), we should enforce these Lie derivatives as follows: $L_{\mathbf{f}}^k h(\mathbf{x})$ ($k = 0, 1, \dots, r$) and $L_{\mathbf{g}}L_{\mathbf{f}}^{r-1} h(\mathbf{x})$. However, the Lie derivatives are computationally expensive because of burdensome higher-order derivatives, see the computation procedure shown by (3). To address this issue, the extended state observer (ESO) is developed in the next section to estimate these Lie derivatives with high accuracy, resulting in the reduction of controller complexity. Furthermore, disturbances can be taken into account to enhance the performance of the controller.

B. Extended State Observer (ESO) Design

Considering the external disturbance and the uncertainties of model parameters, denoted by $w(t)$, the aforementioned r -order cascade integral system in (5) can be rewritten as:

$$\dot{z}_1 = z_2, \dot{z}_2 = z_3, \dots, \dot{z}_r = c(\mathbf{x}, u) + b_0 u + w(t), \quad (8)$$

where $c(\mathbf{x}, u) = a(\mathbf{x}) + (b(\mathbf{x}) - b_0)u$; b_0 is the coefficient describing the influence from u to the cascade integral system.

An ESO treats $d(\mathbf{x}, u) = c(\mathbf{x}, u) + w(t)$ as another variable, which is referred as “overall disturbance.” Thus, for the r -order system (8), the $r+1$ -order ESO is used to estimate $z_1, z_2, \dots, d(\mathbf{x}, u)$. Assuming that the output function of system (8) is the same as that of system (1), i.e., $y = h(\mathbf{x}) = z_1$, the ESO can be expressed as [34]:

$$\begin{cases} e = y - m_1, \\ \dot{m}_1 = m_2 - \beta_{01}g_1(e), \\ \dot{m}_2 = m_3 - \beta_{02}g_2(e), \\ \vdots \\ \dot{m}_r = m_{r+1} - \beta_{0r}g_r(e) + b_0 u, \\ \dot{m}_{r+1} = -\beta_{0,r+1}g_{r+1}(e), \end{cases} \quad (9)$$

where m_1, m_2, \dots, m_{r+1} represent the state variables of ESO; $\beta_{01}, \beta_{02}, \dots, \beta_{0,r+1}$ are the coefficients and $g_{01}(e), g_{02}(e), \dots, g_{0,r+1}(e)$ are nonlinear functions of the error e . Note that ESO takes the error of output y and control input u as the inputs and outputs the values of m_1, m_2, \dots, m_{r+1} , which are the estimates of z_1, z_2, \dots, z_r and overall disturbance $d(\mathbf{x}, u)$, respectively.

Using (7), (8) and (9), we can derive the following nonlinear controller:

$$u = \frac{-m_{r+1} - \sum_{j=1}^r k_j m_j}{b_0}. \quad (10)$$

This controller only relies on the outputs of ESO and thus separates the parameter mismatch error of the original system model. On the other hand, the estimation of overall disturbance m_{r+1} enables the controller to compensate for the system disturbance.

C. Dynamic Modeling of WTG

In this section, both the drivetrain model of WTG and the active power model of wind generator are presented and discussed.

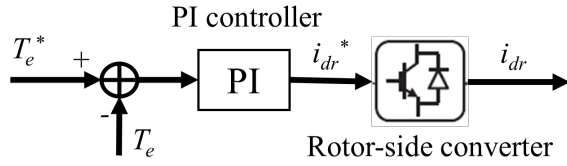


Fig. 1. Scheme of the active power control of the WTG.

1) *Drivetrain Model of WTG*: To investigate the DTTO, we utilize the two-mass drive-train model provided in [35], as follows:

$$\begin{aligned} 2H_{wt}\dot{\omega}_{wt} &= T_m - K_{sh}\theta_{sh} - D_{sh}(\omega_{wt} - \omega_g), \\ 2H_g\dot{\omega}_g &= K_{sh}\theta_{sh} + D_{sh}(\omega_{wt} - \omega_g) - T_e, \\ \dot{\theta}_{sh} &= \omega_B(\omega_{wt} - \omega_g), \end{aligned} \quad (11)$$

2) *Active Power Model of Wind Generator*: This section considers the following conventions: (a) WTG is modeled with a doubly-fed induction generator (DFIG); (b) all variables are referenced to the stator side of generator; (c) the reference dq frame rotates at synchronous angular speed of ω ; (d) the positive power directions of stator and rotor are assumed to be out and into the generator, respectively.

Equations (12) and (13) show the voltage-flux equations of stator and rotor, respectively; (14) and (15) present the corresponding flux-current equations, and the electromagnetic torque is given by (16)

$$\begin{aligned} v_{qs} &= -R_s i_{qs} + \dot{\lambda}_{qs} - \omega \lambda_{ds}, \\ v_{ds} &= -R_s i_{ds} + \lambda_{qs} \dot{\omega} + \omega \lambda_{qs}, \end{aligned} \quad (12)$$

$$\begin{aligned} v_{qr} &= R_r i_{qr} + \dot{\lambda}_{qr} + (\omega - \omega_g) \lambda_{dr}, \\ v_{dr} &= R_r i_{dr} + \dot{\lambda}_{dr} - (\omega - \omega_g) \lambda_{qr}, \end{aligned} \quad (13)$$

$$\begin{aligned} \lambda_{qs} &= -L_s i_{qs} + L_m i_{qr}, \\ \lambda_{ds} &= -L_s i_{ds} + L_m i_{dr}, \end{aligned} \quad (14)$$

$$\begin{aligned} \lambda_{qr} &= L_r i_{qr} - L_m i_{qs}, \\ \lambda_{dr} &= L_r i_{dr} - L_m i_{ds}, \end{aligned} \quad (15)$$

$$T_e = \frac{L_m}{L_s} (\lambda_{qs} i_{dr} - \lambda_{ds} i_{qr}), \quad (16)$$

In the dq reference frame with the stator voltage orientation (SVO), the d -axis is aligned with the stator voltage vector, yielding $v_{ds} = U_s$ and $v_{qs} = 0$. Neglecting stator and rotor resistances, the steady-state stator/rotor voltage equations in SVO frame are obtained from (12): $U_s = v_{ds} \approx \omega \lambda_{qs}$ and $0 = v_{qs} \approx -\omega \lambda_{ds}$, where U_s is the stator voltage magnitude and $\omega = 1$. This yields the approximate expressions of $v_{ds} \approx \lambda_{qs}$ and $\lambda_{ds} = 0$. Therefore, from (16), one has:

$$T_e = \frac{L_m}{L_s} \lambda_{qs} i_{dr}. \quad (17)$$

The active power control diagram of the WTG is shown in Fig. 1, where T_e^* and i_{dr}^* are the reference values of electromagnetic torque and d -axis current of rotor, respectively.

Neglecting converter switching losses, the power balance of the DC bridge between the back-to-back converters is given as:

$$\frac{1}{2C} \frac{d}{dt} v_{dc}^2 = \frac{1}{C} \dot{v}_{dc} v_{dc} = P_i - P_r, \quad (18)$$

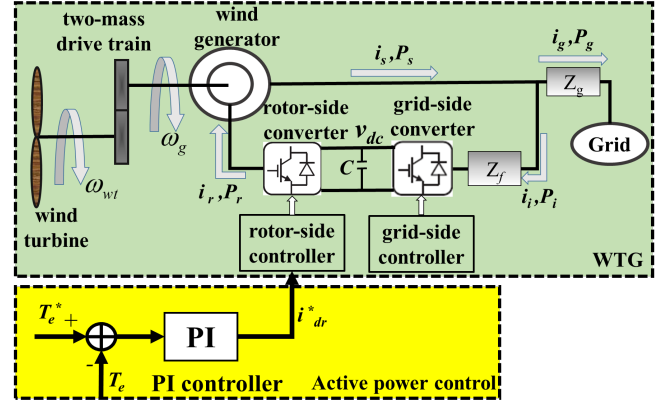


Fig. 2. DFIG-based WTG model.

where P_i and P_r are the active power flowing into the grid-side converter and out from the rotor-side converter, respectively. Generally, the overall scheme of the WTG model is reported in Fig. 2.

3) *Drivetrain Torsional Oscillation of WTG*: A contingency gives raise to the variation of mechanical power or electromagnetic torque of WTG, denoted by ΔT_m and ΔT_e , respectively. Then, the transfer function from ΔT_m or ΔT_e to the torsional angle variation, $\Delta \theta_{sh}$, can be derived from (11), yielding

$$\Delta \theta_{sh} = \frac{\omega_B (H_g \Delta T_m + H_t \Delta T_e)}{2(H_t H_g) s^2 + a H_{tg} s + b H_{tg}} \quad (19)$$

where $H_{tg} = H_t + H_g$, $a = D_{sh} \omega_B$ and $b = K_{sh} \omega_B$. From (19), it can be observed that the variation of mechanical power or electromagnetic torque of WTG may lead to the torsional oscillation of WTG drive train if no damping control is provided. This is because there exists a torsional mode with the natural frequency shown in (20) and the damping coefficient D_{sh} is usually small.

$$\omega_n = \sqrt{\frac{\omega_B K_{sh} H_{tg}}{2H_t H_g}}. \quad (20)$$

D. Proposed Nonlinear Controller of WTG DTTO

If the control input u of DFIG-based WTG is selected as the electromagnetic torque, i.e., a compensation torque $T_{e,Comp}$ is added to the desired electromagnetic torque formulated based on the maximum power point tracking (MPPT) strategy [36] (i.e., $T_{e,MPPT}$), the reference electromagnetic torque T_e^* can be given by:

$$T_e^* = T_{e,MPPT} + u, \quad (21)$$

where $u = T_{e,Comp}$. Then, based on Section II-C, the DFIG-based WTG model is described by a set of nonlinear equations in the form of (1), where the state vector is $\mathbf{x} = [\theta_{sh}, \omega_g, \omega_{wt}, i_{ds}, i_{qs}, i_{dr}, i_{qr}, v_{dc}]^T$ and the input functional vector is $\mathbf{g}(\mathbf{x}) = [0, -\frac{1}{2H_g}, 0, \dots, 0]^T$.

According the controller design procedure in Sections II-A and II-B, selecting the output function is of importance as it determines the Brunovsky standard system in (5), which is the cascade integral system the ESO estimates. Here, we select

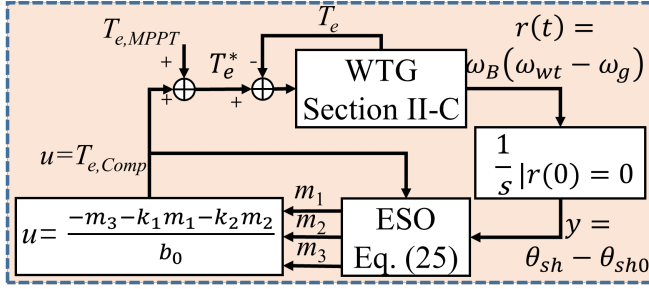


Fig. 3. The proposed nonlinear controller for WTG DTTO.

$y = \theta_{sh} - \theta_{sh,0}$, i.e., the deviation of the torsional angle, as the output. However, the torsional angle is not measurable. Instead, obtaining the measurements of wind turbine and generator rotor speeds ω_{wt} and ω_g is easier to realize in practice. Therefore, based on the third equation of (11), we have the real-time value of the output function from:

$$y = \theta_{sh} - \theta_{sh,0} = \int_0^t r(t) dt, \quad (22)$$

where $r(t) = \omega_B(\omega_{wt} - \omega_g)$ and the initial value of integration $r(0)$ is zero.

Based on (2), we have $r = 2$ since:

$$\begin{cases} L_g L_f (\theta_{sh} - \theta_{sh,0}) = \frac{\omega_B}{2H_g}, \\ L_g (\theta_{sh} - \theta_{sh,0}) = 0. \end{cases} \quad (23)$$

Combining (4) and (5) with the WTG model and considering its disturbance in the form of (8), we can also obtain the partial exactly linearized system of the WTG in the form of (5), shown as:

$$\begin{cases} \dot{z}_1 = z_2 = \omega_B(\omega_{wt} - \omega_g), \\ \dot{z}_2 = d(\omega_g, \omega_{wt}, \theta_{sh}, u) + b_0 u, \\ \dot{z}_i = \varphi_i(\mathbf{x}) \quad i = 3, 4, \dots, 8, \end{cases} \quad (24)$$

where $b_0 = \frac{\omega_B}{2H_g}$; the overall disturbance of the WTG $d(\omega_g, \omega_{wt}, \theta_{sh}, u) = c(\omega_g, \omega_{wt}, \theta_{sh}, u) + w(t)$, $c(\omega_g, \omega_{wt}, u)$ can be obtained based on (8); $w(t)$ is the disturbance of the WTG model; $\varphi_i(\mathbf{x}) = x_i - x_{i,0}$; x_i and $x_{i,0}$ are the i -th state variable of the WTG and the corresponding initial value, respectively. Note that they satisfy $L_g \varphi_i(\mathbf{x}) = 0$, $i = 3, 4, \dots, 8$. This is because

$$L_g \varphi_i(\mathbf{x}) = \frac{\partial \varphi_i(\mathbf{x})}{\partial \mathbf{x}^T} \mathbf{g}(\mathbf{x}),$$

$$\frac{\partial \varphi_i(\mathbf{x})}{\partial \omega_g} = 0, \quad i = 3, 4, \dots, 8.$$

Therefore, by taking the torsional angle deviation (22) and control input u as inputs, a third-order ESO in the form of (9) can be adopted to estimate the state variables z_1, z_2 and the overall disturbance $d(\omega_g, \omega_{wt}, \theta_{sh}, u)$ of the WTG model (24). Formally, we have

$$\begin{cases} e = m_1 - z_1, \\ \dot{m}_1 = m_2 - \beta_{01}e, \\ \dot{m}_2 = m_3 - \beta_{02}\zeta(e, \alpha_1, \delta) + b_0 u, \\ \dot{m}_3 = -\beta_{03}\zeta(e, \alpha_2, \delta), \end{cases} \quad (25)$$

The nonlinear function $\zeta(e, \alpha, \delta)$ is expressed by:

$$\zeta(e, \alpha, \delta) = \begin{cases} \frac{e}{\delta^{1-\alpha}} & |e| < \delta, \\ \text{sign}(e) |e|^\alpha & |e| \geq \delta, \end{cases} \quad (26)$$

where α and δ are two parameters and the sign function outputs 1, 0 and -1 for positive value, zero and negative values, respectively. The interested reader can find more details on the performance verification of ESO in [22].

Finally, according to (10), the proposed nonlinear controller for WTG DTTO can be derived as follows:

$$T_{e,Comp} = u = \frac{-m_3 - k_1 m_1 - k_2 m_2}{b_0}. \quad (27)$$

The complete control diagram of the proposed nonlinear controller for WTG DTTO is shown in Fig. 3, i.e., the closed-loop system.

E. Stability and Robustness of the Closed-loop System

As discussed in Section II-A, the stability of the closed-loop system is related to the differential geometry theory. The performance of ESO (25) has been validated in [22]. Consider $z_1 = \theta_{sh} - \theta_{sh,0}$ and $z_2 = \dot{z}_1 = \omega_B(\omega_{wt} - \omega_g)$ as two output variables, denoted by y_1 and y_2 , respectively. The objective values of the output variables are y_{1r} and y_{2r} and should be as close as possible to y_1 and y_2 respectively. Specifically, the idea of differential geometry theory based controller is to find a control input u that can achieve $\lim_{t \rightarrow \infty} |y_1 - y_{1r}| = 0$ and $\lim_{t \rightarrow \infty} |y_2 - y_{2r}| = 0$. The control quantity u can be obtained from (1) to (7). It is interesting to note that the proposed controller is consistent with the idea of the nonlinear control with objective holographic feedbacks and its stability of the closed-loop system is given in [37]. The procedures to set up the proposed controller by objective holographic feedbacks theory-based nonlinear control are as follows:

1) Construct a Brunovsky system:

$$\begin{bmatrix} \dot{y}_1 - \dot{y}_{1r} \\ \dot{y}_2 - \dot{y}_{2r} \end{bmatrix} = \begin{bmatrix} 0 & 1 \\ 0 & 0 \end{bmatrix} \begin{bmatrix} y_1 - y_{1r} \\ y_2 - y_{2r} \end{bmatrix} + \begin{bmatrix} 0 \\ 1 \end{bmatrix} v, \quad (28)$$

where $v = \dot{y}_2 - \dot{y}_{2r}$ and $\dot{y}_2 = L_f \omega_B(\omega_{wt} - \omega_g) + L_g \omega_B(\omega_{wt} - \omega_g) = F(\mathbf{x}) + \frac{\omega_B}{2H_g} u$; $F(\mathbf{x})$ can be expressed as $\frac{\omega_B T_m}{2H_{wt}} + \frac{\omega_B T_{MPPT}}{2H_g} + (\frac{\omega_B}{2H_{wt}} + \frac{\omega_B}{2H_g})(K_{sh} \theta_{sh} + D_{sh}(\omega_{wt} - \omega_g))$.

2) The Brunovsky system (28) is a completely controllable linear system. Then, an optimal control, i.e. the linear quadratic control proposed in [33], can be applied to obtain v , yielding:

$$v = \sum_{k=1}^m -k_i I_i. \quad (29)$$

3) Equations (28) and (29) lead to the following control strategy u :

$$u = \frac{-\sum_{i=1}^2 k_i (y_i - y_{ir}) - F(\mathbf{x}) + \dot{y}_{2r}}{\frac{\omega_B}{2H_g}}. \quad (30)$$

The stability of the closed-loop system can be easily proved following the procedure in [37]. [34], [38] show that a controller designed for the nominal system can be robustified by an ESO. This is because ESO can effectively estimate the

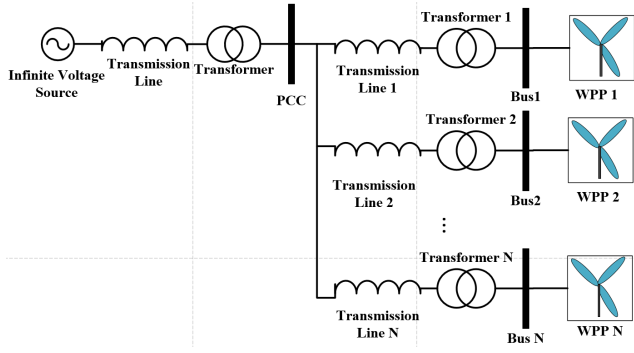


Fig. 4. The schematic diagram of the wind power plants integrated power system.

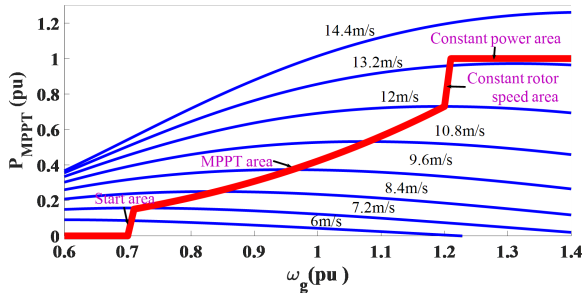


Fig. 5. The MPPT power-speed curve of DFIG.

dynamic states as well as the effects of uncertainties and disturbances instead of identifying their mathematical expressions [22]. This guarantees the robustness of the proposed controller that strategically integrates differential geometry theory with ESO. In this paper, “robustness” means the capacity of dealing with the uncertainty of parameters H_t , H_g , K_{sh} and D_{sh} as well as the large external disturbance of the wind power integrated system. The external disturbance includes the electromagnetic power disturbance caused by grid fault or the mechanical power disturbance resulted from the instantaneous wind speed variation.

III. CASE STUDY

The case study consists of two parts. A power system with simplified-model small-capacity WPPs is considered in Section III-A. Then, a power system with detailed-model large-capacity power WPPs is tested in Section III-B.

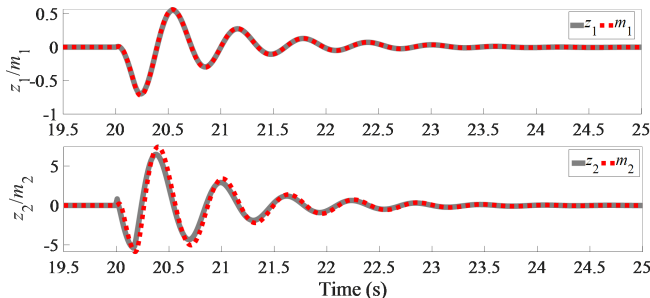


Fig. 6. The state estimation results by ESO on the partially linearized system of WTG.

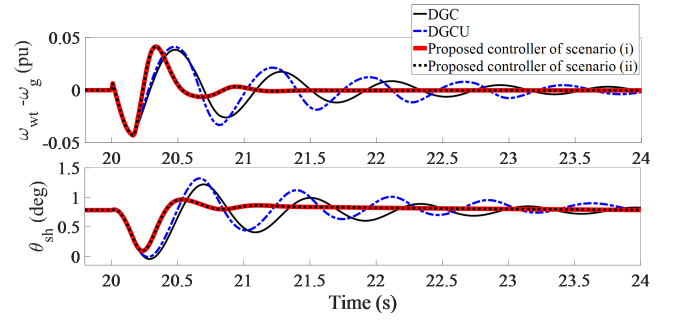


Fig. 7. The responses of the relative angular speed and torsional angle for different controllers.

A. System with Simplified-Model Small-Capacity WPPs

This section aims at demonstrating the effectiveness, robustness and advantages of the proposed controller for the mitigation of WTG DTTO under various large disturbance conditions. The scheme of the power system is presented in Fig. 4, where N denotes the number of WPPs. Each WPP consists of 6 DFIG-based WTGs with 1.5 MW rated power for each DFIG. Each WPP is modelled as an aggregated WTG model. A conventional linear controller (LC), i.e., approximate linearization-based controller, and a nonlinear controller based on sliding-mode control (SMC) [21] are also considered for comparisons. Table I shows the parameters for the DFIG and the proposed controller. Figure 5 shows the MPPT power-speed curve of the DFIG. The electromagnetic torque compensation of LC is given by:

$$T_{e,Comp} = l_1 \Delta \omega_{wt} + l_2 \Delta \omega_g + l_3 \Delta \theta_{sh}, \quad (31)$$

where $l_1 = 2.2302$, $l_2 = -1.3407$ and $l_3 = -0.0304$ are the coefficients of state feedback controller for the approximately linearized WTG drive-train system. These parameters can be calculated on the basis of linear quadratic optimal theory.

TABLE I
PARAMETERS FOR THE DFIG AND PROPOSED CONTROLLER

DFIG			
H_g	0.685 s	H_t	4.32 s
K_{sh}	1.1 pu/rad	p	3
R_s	0.023 pu	L_s	0.18 pu
R_r	0.016 pu	L_r	0.16 pu
V_{cutin}	4 m/s	V_{rated}	13.4 m/s
		V_{cutout}	25 m/s
		D_{sh}	1.5
		ω_B	377/3 rad/s
		L_m	2.9 pu
		ω	377 rad/s
Proposed controller			
β_{01}	100	β_{02}	3000
α_1	0.9	α_2	0.3
k_1	1	k_2	1.7321
		β_{03}	5000
		δ	0.1

This section is organized as follows. Section III-A1 validates the effectiveness and the robustness of the proposed controller against parameter uncertainties via the comparisons with differential geometry-based nonlinear controller (DGC). Section III-A2 considers a single WPP and investigates the advantages of the proposed controller over the LC and SMC under different wind speeds and various disturbances. Comparison results for multiple WPPs are shown in Section III-A3 to demonstrate the scalability of the proposed controller. All the simulations are implemented in Matlab/Simulink.

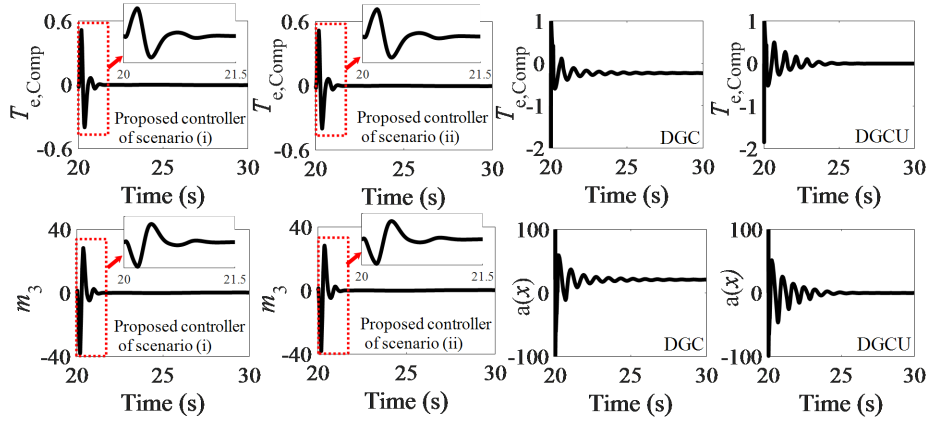


Fig. 8. The compensation torques provided by proposed controller, DGC and DGPU.

1) *Robustness to Parameter Uncertainty*: In this example, we assume there is a single WPP connected power system. A three-phase fault occurs at $t = 20$ s on the Bus 1 of the grid shown in Fig. 4 and is cleared at $t = 20.15$ s. The wind speed is 15 m/s. Both DGC and the proposed controller are implemented to damp DTTO in the following two scenarios: (i) the drivetrain parameters of DFIG H_g , H_t , D_{sh} and K_{sh} are the same as the true values shown in Table I; and (ii) parameter uncertainties exist, where it is assumed that the used parameters are 80% of each true value. DGPU means the DGC considering parameter uncertainties. The states z_1 and z_2 obtained from the differential geometry and their estimations m_1 and m_2 by ESO are shown in Fig. 6. Fig. 7 shows the responses of the relative angular speed and torsional angle for different methods. The compensation torques provided by proposed controller, DGC and DGPU are given in Fig. 8.

Figure 6 shows that the estimated m_1 and m_2 match quite well with the actual values, i.e., z_1 and z_2 , confirming the high estimation accuracy of ESO for the partially linearized WTG model. The maximum relative estimation errors of z_1 and z_2 are 0.0096% and 1.23%, respectively. The responses of relative angular speed and torsional angle in Fig. 7 indicate that, independently from parameter uncertainty, the proposed controller can achieve the desired performance of damping DTTO. Furthermore, the DGC does not deal well with strong drive-train oscillation and its performance worsens with parameters uncertainty (see the response of the DGPU). This is because the proposed controller relies on the outputs of ESO but does not depend directly on drive-train parameters. While the DGC is determined based on the drive-train parameters and, hence, it is sensitive to the uncertainty of such parameters.

The choice of the control input is crucial for the performance of a controller. In this case, the control input is the compensation torque $T_{e,Comp}$. Taking a closer look at Fig. 8, the compensation torque of the proposed controller shows less oscillations than the DGC and DGPU. It is interesting to note that the proposed controller and DGC strongly depend on the transient behavior of m_3 (the estimation of the overall disturbance of the WTG) and $a(x)$, respectively. With this regard, m_3 and $a(x)$ are consistent with the $T_{e,Comp}$ trajectories of

the proposed controller and DGC. The derivations in Section II show that m_3 and $a(x)$ lead to the main differences between the proposed controller and DGC. As Fig. 6 has verified the high estimation accuracy of z_1 and z_2 , m_3 and $a(x)$ become the critical quantities for the proposed controller and DGC, respectively. Furthermore, during the up-swing of the relative angular speed and torsional angle in Fig. 7, all trajectories of $T_{e,Comp}$ in Fig. 8 are in the opposite of the corresponding swings. This is due to the fact that the proposed controller, DGC and DGPU aim at making the oscillations of θ_{sh} and $\omega_B(\omega_{wt} - \omega_g)$ to be as close to θ_{sh0} and 0 as possible, respectively.

2) *Robustness to Different Wind Speeds and Disturbances*: Two types of large disturbances are considered in this section: (i) a three-phase fault, same as the one considered in Section III-A1; and (ii) wind speed variations. For the fault, two wind speeds are considered, namely, 15 m/s and 10 m/s. In the second scenario, the wind speed is initially equal to 15 m/s and then a sudden increment of 5 m/s from $t = 20$ s to $t = 23$ s occurs. Since LC has poor performance of handling large disturbance, only the comparisons between SMC and our proposed controller are specifically analyzed.

a) *Three-phase fault*: Figure 9 shows the responses of the relative angular speed and torsional angle for 15 m/s wind speed, where the responses of relative angular speed with SMC and proposed controller are particularly displayed in Fig. 10. The critical quantities, i.e., $a(x)$ for the proposed controller and δ for SMC [21] are given in Fig. 11. Fig. 12 shows the responses of the relative angular speed and torsional angle when the wind speed is 10 m/s.

Figure 9 reveals that LC has a poor performance of suppressing WTG DTTO as the truncation error for the approximate linearization is large in the presence of large disturbance; SMC can reduce the oscillation frequency and magnitude to a certain extent; by contrast, the proposed controller achieves even better performance, including lower oscillation magnitude and faster damping speed. A closer look at Fig. 10 shows that the oscillations last for about 10 s with SMC while 2 s with proposed controller, thus, the proposed controller achieves 5 times the damping of SMC. Thanks

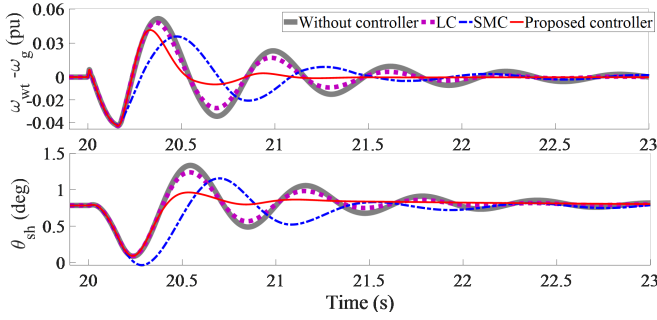


Fig. 9. Trajectories of the relative angular speed and torsional angle following a three-phase fault and wind speed equal to 15 m/s.

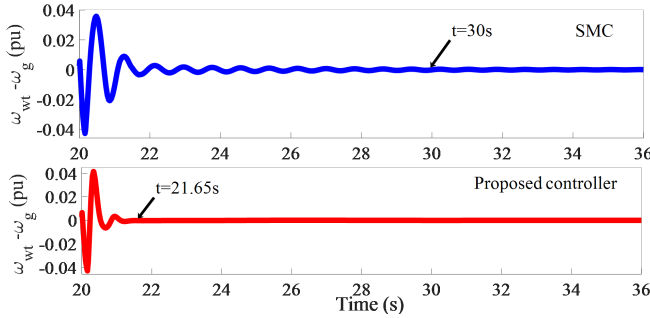


Fig. 10. Trajectories of the relative angular speed for SMC and proposed controller following a three-phase fault and wind speed equal to 15 m/s.

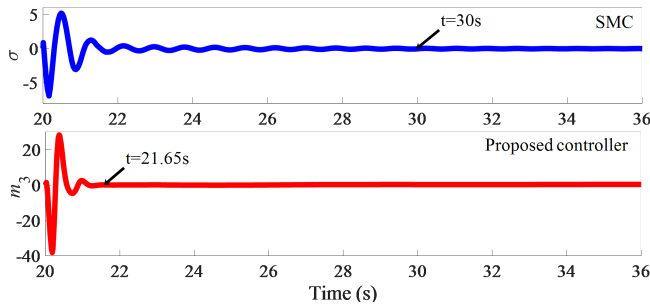


Fig. 11. Critical quantities of SMC and proposed controller following a three-phase fault and wind speed equal to 15 m/s.

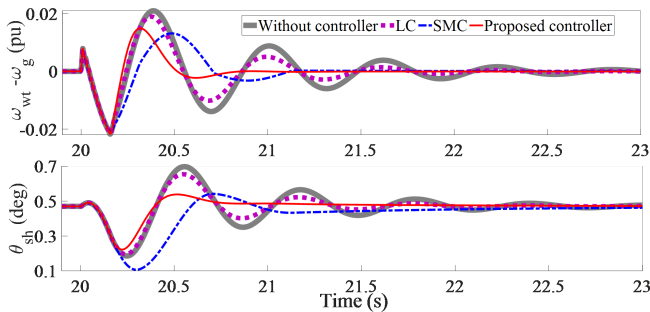


Fig. 12. Trajectories of the relative angular speed and torsional angle following a three-phase fault and wind speed equal to 10 m/s.

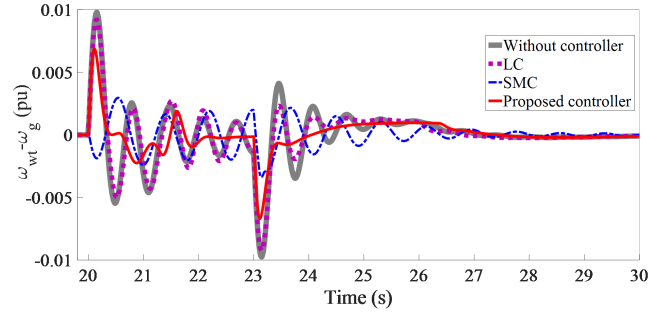


Fig. 13. Trajectories of the relative angular speed following a wind speed disturbance.

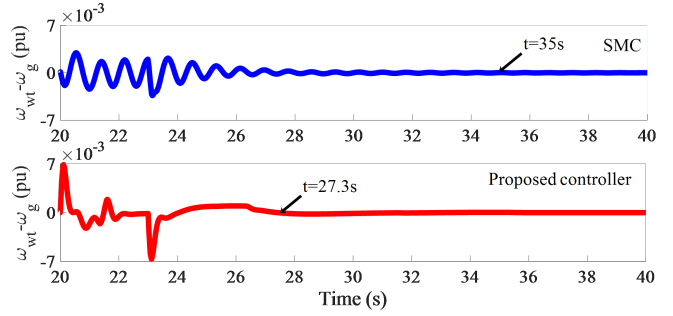


Fig. 14. Trajectories of the relative angular speed with SMC and proposed controller following a wind speed disturbance.

to the ESO, similar to the discussion provided in Section III-A-1), the critical quantities determine the performances of compensation torques of SMC and proposed controller, and better compensation torques can lead to better control performances with respect to WTG DTTO, see Fig. 11 for details. Fig. 12 also confirms those conclusions for the scenario with wind speed equal to 10 m/s.

b) Wind Speed Disturbance: The trajectories of the relative angular speed for different controllers are shown in Fig. 13. The results related to proposed controller and SMC and their critical quantities are presented in Fig. 14 and Fig. 15, respectively. When encountering wind speed disturbance, Fig. 13 shows that the proposed controller can effectively damp WTG DTTO with lower oscillation frequency and higher recovery efficiency than LC and SMC controllers. Again, LC has the poorest performance in handling these scenarios.

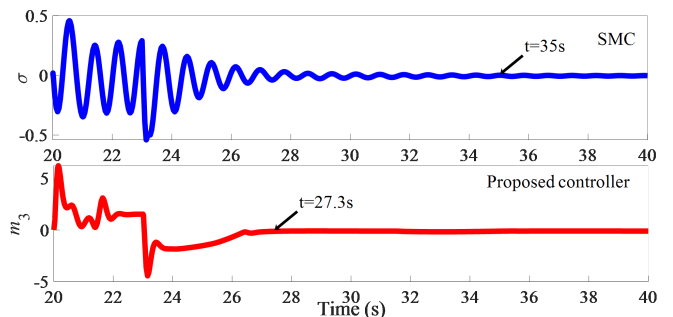


Fig. 15. Critical quantities of SMC and proposed controller following a wind speed disturbance.

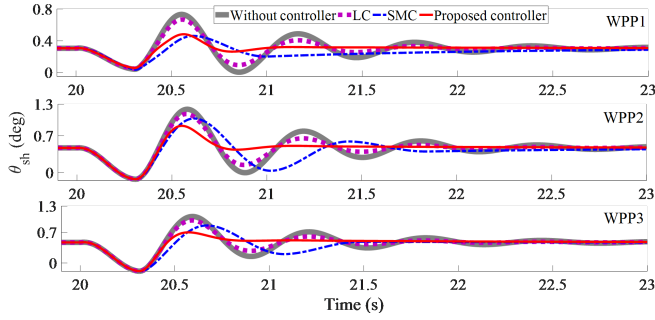


Fig. 16. Comparing trajectories of the torsional angle of the WTG drive train for multiple WPPs.

Figures 14 and 15 also show that the proposed controller can reach the steady-state condition at 27.3 s while SMC has an unsatisfactory performance with higher oscillation frequency and longer oscillation periods, which lasts until about 35 s. It is also interesting to point out that the proposed controller can reach at another steady state in the duration of disturbance, i.e., 20 s to 23 s, while the alternatives fail to do so, see Fig. 13 to Fig. 15.

3) Extension to Multiple WPPs Integrated Power System:

This section demonstrates the scalability of the proposed controller for multiple WPPs. In this case, we consider the system with three WPPs, as shown in Fig. 4 and a three-phase fault occurs at the point of common coupling (PCC) at $t = 20$ s and is cleared at $t = 20.3$ s. The wind speeds of WPP1, WPP2 and WPP3 are 8 m/s, 10 m/s and 10 m/s, respectively, and the transmission line distances of each WPP with respect to the PCC are 50 km, 35 km and 10 km. The positive resistance, inductance and capacitance of transmission each line are $0.1153 \Omega/\text{km}$, $1.05 \cdot 10^{-3} \text{ H}/\text{km}$ and $11.33 \cdot 10^{-9} \text{ F}/\text{km}$, respectively. The corresponding negative resistance, inductance and capacitance are $0.413 \Omega/\text{km}$, $3.32 \cdot 10^{-3} \text{ H}/\text{km}$ and $5.01 \cdot 10^{-9} \text{ F}/\text{km}$.

The trajectories of each WPP torsional angle for different control strategies are displayed in Fig. 16. These trajectories show that the LC cannot properly damp the WTG DTTO and its response curve is similar to the original one without control. It is interesting to notice that compared with the previous scenarios, the oscillation magnitudes for SMC and the proposed controller are close. However, SMC still needs a much longer time to damp out the oscillations as compared to our controller. The general conclusion is consistent with what we have observed before, i.e., LC has poor performance for DTTO in the presence of large disturbance; SMC has improved performance over LC but it takes longer time to damp out the oscillations as compared to our proposed controller; and the proposed controller has the smallest oscillation frequency.

B. Results with Detailed-Model Large-Capacity WPPs

This section further illustrates the advantages of the proposed controller through simulations based on WPPs with large capacity, i.e., 90 MW, and detailed model. The schematic diagram is shown in Fig. 17, where the wind speed direction is assumed to be perpendicular to the column of WPP. Therefore, each column can be modeled as an aggregated WTG consist-

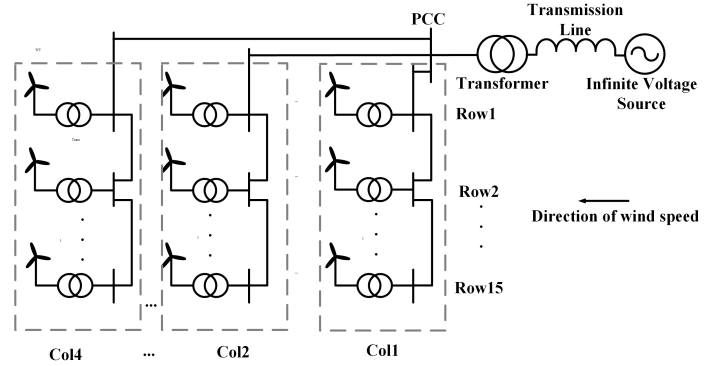


Fig. 17. The schematic diagram of grid with detailed-model and high-power WPPs.

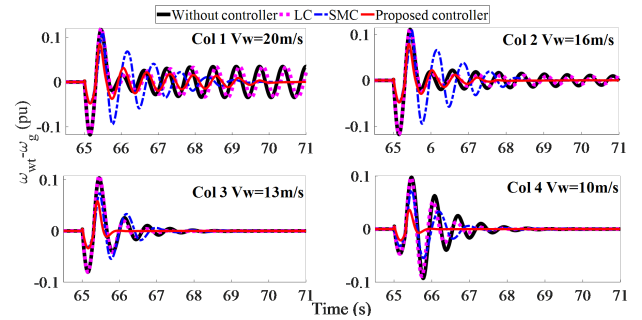


Fig. 18. Trajectories of the relative angular speed in different columns of WPPs.

ing 15 DFIGs. The cable distance between two consequent columns is 882 m and the length of the transmission line is 20 km. The parameters of the cables and the transmission lines are assumed to be the same as those in Section III-A3. Considering the wake effect of wind power, the wind speeds of each column are 20 m/s, 16 m/s, 13 m/s and 10 m/s, respectively. A three-phase fault occurs at the end of the transmission line at 65 s and is cleared at 65.3 s.

Figure 18 shows that the proposed controller achieves much better performance in suppressing DTTOs of all aggregated WTGs than other methods. Note that without damping controller, DTTO is particularly serious with wind speeds in the constant power area, i.e., 20 m/s and 16 m/s. The system even losses stability under 20 m/s wind speed, while WTG working in MPPT area (i.e., 10 m/s) has a stronger capability of damping DTTO. The best damping can be observed under 13 m/s wind speed, which belongs to the constant rotor speed area. These results are consistent with those discussed in [10] and can be explained as follows: the damping of DTTOs increases with the slope of the power-speed curve shown in Fig. 5. Note that the slope of the curve in constant power area is null, whereas the maximum slope occurs in the constant rotor speed area. In terms of suppressing DTTOs under different areas, the proposed controller outperforms the solution based on LC and SMC and leads to overall smaller oscillations. The consistent conclusions with that of Section III-A can be drawn in this section, further demonstrating the scalability of the proposed controller.

IV. CONCLUSIONS AND FUTURE WORK

The paper proposes a novel nonlinear controller to damp WTG DTTO originated by large disturbances. The proposed controller integrates differential geometry and ESO. In particular, the differential geometry serves to transform the nonlinear equations of the WTG system into a simple second-order Brunovsky system. Then, ESO allows estimating the states of the transformed system. The resulting controller proves to effectively compensate the oscillations caused by the disturbances and, thanks to the ESO, to be robust with respect to model parameter uncertainty. Simulation results show that the proposed controller performs better than conventional linear and nonlinear controllers, i.e., shows higher damping under all considered disturbances and wind speed operating conditions.

Future work will focus on exploiting differential geometry to develop novel nonlinear controllers and investigating the benefits of using battery energy storage for damping WTG DTTO following large disturbances. We also aim at validating the proposed control strategy using experimental data and/or hardware-in-the-loop simulations.

REFERENCES

- [1] Y. Zhao, L. Ye, W. Wang, et al, "Data-driven correction approach to refine power curve of wind farm under wind curtailment," *IEEE Trans. Sustain. Energy*, vol. 9, no. 1, pp. 95–105, 2018.
- [2] T. Ackerman, "Wind power in power systems," *2nd Edition*. Wiley, 2005.
- [3] A. Tabesh, R. Irvani, "Transient behaviour of a fixed-speed grid-connected wind farm," *In: Proc. Int. Conf. Power Systems Transients, Montreal, Canada*, 2005.
- [4] G. Ramtharan, N. Jenkins, O. Anaya-Lara, E. Bossanyi, "Influence of rotor structural dynamics representations on the electrical transient performance of FSG and DFIG wind turbines," *Wind Energy*, vol. 10, pp. 293–301, 2007.
- [5] L. Chen, H. Xu, J. Wenske, "Active damping of torsional vibrations in the drive train of a DFIG wind turbine," *In: Proc. Int. Conf. Renew. Energies and Power Quality, Cordoba, Spain*, 2014.
- [6] S.M. Muyeen, M.H. Ali, R. Takahashi, T. Murata, "Blade-shaft torsional oscillation minimization of wind turbine generator system by using STATCOM/ESS," *In: Proc. power tech. conf., Lausanne*, 2007.
- [7] Z. Xing, L. Liang, H. Guo, X. Wang, "Damping control study of the drive train of DFIG wind turbine," *In: Proc. int. conf. energy and environment technology, Guilin, Guangxi*, 2009.
- [8] M. Garmroodi, G. Verbic, D. J. Hill, "Frequency support from wind turbine generators with a time variable droop characteristic," *IEEE Trans. Sustain. Energy*, vol. 9, no. 2, pp. 676–684, 2018.
- [9] X. Zhang, W. He, J. Hu, "Impact of inertia control of DFIG-based WT on torsional vibration in drive train," *IEEE Trans. Sustain. Energy*, 2020, in press.
- [10] M. Rahimi, "Improvement of energy conversion efficiency and damping of wind turbine response in grid connected DFIG based wind turbines," *Int J Elec Power*, vol. 95, pp. 11–25, 2018.
- [11] H. A. Mohammadpour, Y. Shin, and E. Santi, "SSR analysis of a DFIG based wind farm interfaced with a gate controlled series capacitor," *IEEE Applied Power Electronics Conf. & Exp.*, pp. 3110–3117, 2014.
- [12] H. Xie, B. Li, C. Heyman, M. M. de oliveira, M. Monge, "Subsynchronous resonance characteristic in presence of doubly-fed induction generator and series compensation and mitigation of subsynchronous resonance by proper control of series capacitors," *IET Renew. Power Gener.*, vol. 8, no. 4, pp. 411–421, 2014.
- [13] E. Bossanyi, "Wind turbine control for load reduction," *Wind Energy*, vol. 6, no. 3, pp. 229–244, 2003.
- [14] J. Licari, C. E. Ugalde-Loo, J. B. Ekanayake, et al, "Damping of torsional vibrations in a variable-speed wind turbine," *IEEE Trans. Energy Convers.*, vol. 28, no. 1, pp. 172–180, 2013.
- [15] I. P. Girsang, J. S. Dhupia, E. Muljadi, et al, "Modeling and control to mitigate resonant load in variable-speed wind turbine drive train," *IEEE J. Emerg. Sel. Topics Power Electron.*, vol. 1, no. 4, pp. 277–286, 2013.
- [16] G. Mandic, A. Nasiri, E. Muljadi, F. Oyague, "Active torque control for gearbox load reduction in a variable-speed wind turbine," *IEEE Trans. Industry Appl.*, vol. 48, no. 6, pp. 2424–2432, 2012.
- [17] M. Neshati, T. Jersch, J. Wenske, "Model based active damping of drive train torsional oscillations for a full-scale wind turbine nacelle test rig," *in Proc. Amer. Control Conf., Boston, MA, USA*, 2016.
- [18] T. Jain, and J. J. Yamé, "Fault-tolerant economic model predictive control for wind turbines," *n, IEEE Trans. Sustain. Energy*, vol.10, no.4, pp.1696–1704, 2018.
- [19] X. Xi, H. Geng, G. Yang, et al, "Torsional oscillation damping control for DFIG-based wind farm participating in power system frequency regulation," *IEEE Trans. Ind. Appl.*, vol.54, no.4, pp. 3687–3701, 2018.
- [20] X. Xi, H. Geng, G. Yang, et al, "Two-Level Damping Control for DFIG-based Wind Farm Providing Synthetic Inertial Service," *IEEE Trans. Ind. Appl.*, vol.54, no.2, pp. 1712–1723, 2017.
- [21] F. Fateh and W. N. White and D. Gruenbacher, "Torsional Vibrations mitigation in the drive train of DFIG-based grid-connected wind turbine," *IEEE Trans. Ind. Appl.*, vol. 53, no. 6, pp. 5760–5767, 2017.
- [22] W. Wang, Z. Gao, "A comparison study of advanced state observer design techniques," *American Control Conference. IEEE*, 2003.
- [23] G. Chen, "Stability of Nonlinear Systems," *Research Studies Press.*, 2005.
- [24] M. Spivak, "A comprehensive introduction to differential geometry," *Publish or Perish, inc.*, 1997.
- [25] A. Isidori, "Nonlinear Control Systems: An Introduction[M]," *Springer-Verlag*, 1985.
- [26] T. J. Tarn, A. K. Bejczy, A. Isidori and Y. Chen, "Nonlinear feedback in robot arm control," *The 23rd IEEE Conference on Decision and Control*, Las Vegas, Nevada, USA, pp. 736–751, 1984.
- [27] G. Meyer, R. Su, L. R. Hunt, "Application of nonlinear transformations to automatic flight control," *Automatica*, vol.20, no.1, pp-103–107, 1984.
- [28] Q. Lu, Y. Z. Sun, "Nonlinear stabilizing control of multimachine systems," *IEEE Tran. Power Syst.*, vol.4, no.1, pp: 236–241, 1989.
- [29] Q. Lu, Y. Z. Sun, "Decentralized nonlinear optimal excitation control," *IEEE Tran. Power Syst.*, vol.11, no.4, pp: 1957–1962, 1996.
- [30] B. Wang, Y. Xu, Z. Shen, J. Zou, C. Li and H. Liu, "Current control of grid-connected inverter with LCL filter based on extended-state observer estimations using single sensor and achieving improved robust observation dynamics," *IEEE Trans. Ind. Electron.*, vol. 64, no. 7, pp. 5428–5439, 2017.
- [31] H. Khalil, "Nonlinear systems," Prentice-Hall, 1996.
- [32] M. Vidyasagar, "Nonlinear Systems Analysis," Prentice-Hall, 1992.
- [33] T. Geerts, "A priori results in linear-quadratic optimal control theory," *IEEE Trans. Autom. Control*, vol.8, no.1, pp:56–59, 1991.
- [34] S. E. Talole, A. A. Godbole, J. P. Kolhe, et al, "Robust Roll Autopilot Design for Tactical Missiles," *J Guid. control Dynam.*, vol.34, no.1, pp.107–117, 2011.
- [35] H. Geng, X. Xi, L. Liu, et al, "Hybrid modulated active damping control for DFIG based wind farm participating in frequency response," *IEEE Trans. on Energy Convers.*, vol. 32, no. 3, pp. 1220–1230, 2017.
- [36] Z. Chen, M. Yin, Y. Zou, K. Meng, Z. Dong, "Maximum wind energy extraction for variable speed wind turbines with slow dynamic behavior," *IEEE Trans. Power Syst.*, vol. 32, no. 4, pp. 3321–3322, 2017.
- [37] L. Hui, W. Ni, W. Hua, X. Li, "Nonlinear excitation control with objective holographic feedbacks," *Adv. Math.*, vol. 218, no. 4, pp. 1–7, 2008.
- [38] B. Panchal, J. W. P. Kolhe, S. E. Talole, "Robust predictive control of a class of nonlinear systems," *J Guid. control Dynam.*, vol.37, no.5, pp.1437–1445, 2014.



Bi Liu was born in Sichuan province, P.R. China. She received the B.M. degree in Industrial Engineering in School of Business Administration from Sichuan University (SCU) in 2009, and now works on a Ph.D degree in Control Science and Engineering in School of Mechanical and Electrical Engineering from University of Electronics Science and Technology of China (UESTC). Her main research direction includes uncertainty quantification on power flow, renewable energy integrated power system stability control and auxiliary frequency regulation on power system with renewable energies.

Estimation and IEEE Task Force on Cyber-Physical Interdependency for Power System Operation and Control, co-chair of IEEE Working Group on Power System Static and Dynamic State Estimation, and the Secretary of the IEEE Task Force on Synchronphasor Applications in Power System Operation and Control.



Junbo Zhao (SM'19) is currently an Assistant Professor at Mississippi State University, Starkville, MS, USA. He received the Ph.D. degree in Electrical Engineering from the Department of Electrical and Computer Engineering, Virginia Tech, Blacksburg, VA, USA, in 2018. He was a Research Assistant Professor at Virginia Tech from May 2018 to August 2019. He did the summer internship at Pacific Northwest National Laboratory from May to August 2017. He is currently the chair of IEEE Task Force on Power System Dynamic State and Parameter

Estimation and IEEE Task Force on Cyber-Physical Interdependency for Power System Operation and Control, co-chair of IEEE Working Group on Power System Static and Dynamic State Estimation, and the Secretary of the IEEE Task Force on Synchronphasor Applications in Power System Operation and Control.

He has published three book chapters and more than 90 peer-reviewed journal and conference papers. His research interests are cyber-physical power system modeling, estimation, security, dynamics and stability, uncertainty quantification, robust statistical signal processing and machine learning for smart grid. He serves as the editor of IEEE Transactions on Power Systems, IEEE Transactions on Smart Grid and IEEE Power and Engineering Letters, the Associate Editor of International Journal of Electrical Power Energy Systems, and the subject editor of IET Generation, Transmission & Distribution. He is the receipt of best paper awards of 2020 IEEE PES General Meeting and 2019 IEEE PES ISGT Asia.



Qi Huang (S'99, M'03, SM'09) was born in Guizhou province in the People's Republic of China. He received the B.S. degree from Fuzhou University, 856 Fuzhou, China, in 1996, the M.S. degree from 857 Tsinghua University, Beijing, China, in 1999, and the Ph.D. degree from Arizona State University, Tempe, AZ, USA, in 2003, all in Electrical Engineering. He is currently a professor at UESTC, the Executive Dean of School of Energy Science and Engineering, UESTC, and the director of Sichuan State Provincial Lab of Power System Wide-area

Measurement and Control. He is a member of IEEE since 1999. His current research and academic interests include power system instrumentation, power system monitoring and control, and power system high performance computing.



Federico Milano (F'16) received from the Univ. of Genoa, Italy, the ME and Ph.D. in Electrical Eng. in 1999 and 2003, respectively. From 2001 to 2002, he was with the Univ. of Waterloo, Canada, as a Visiting Scholar. From 2003 to 2013, he was with the Univ. of Castilla-La Mancha, Spain. In 2013, he joined the Univ. College Dublin, Ireland, where he is currently Prof. of Power Systems Control and Protections and Head of Elec. Eng. His research interests include power system modeling, control and stability analysis.



Weihao Hu (S'06, M'13, SM'15) received the B.Eng. and M.Sc. degrees from Xi'an Jiaotong University, Xi'an, China, in 2004 and 2007, respectively, and Ph. D. degree from Aalborg University, Denmark, in 2012, all in Energy Technology. He is currently a Full Professor and the Director of Institute of Smart Power and Energy Systems (IS-PES) at the University of Electronics Science and Technology of China (UESTC). He was an Associate Professor at the Department of Energy Technology, Aalborg University, Denmark and the Vice Program

Leader of Wind Power System Research Program at the same department. His research interests include artificial intelligence in modern power systems and renewable power generation.

He has led/participated in more than 15 national and international research projects and he has more than 170 publications in his technical field. He is an Associate Editor for IET Renewable Power Generation, a Guest Editor-in-Chief for Journal of Modern Power Systems and Clean Energy Special Issue on Applications of Artificial Intelligence in Modern Power Systems, a Guest Editor-in-Chief for Transactions of China Electrical Technology Special Issue on Planning and operation of multiple renewable energy complementary power generation systems, and a Guest Editor for the IEEE TRANSACTIONS ON POWER SYSTEM Special Section on Enabling very high penetration renewable energy integration into future power systems. He was serving as the Technical Program Chair (TPC) for IEEE Innovative Smart Grid Technologies (ISGT) Asia 2019 and is serving as the Conference Chair for the Asia Energy and Electrical Engineering Symposium (AEEES 2020). He is currently serving as Chair for IEEE Chengdu Section PELS Chapter and he is an IEEE Senior Member.